The HKU Scholars Hub   The University of Hong Kong   香港大學學術庫

Title	**Effects of magnetic coupling of nonadjacent resonators on wireless power domino-resonator systems**
Author(s)	**Lee, CK; Zhong, WX; Hui, SYR**
Citation	**IEEE Transactions on Power Electronics, 2012, v. 27 n. 4, p. 1905-1916**
Issued Date	**2012**
URL	**http://hdl.handle.net/10722/155734**
Rights	**IEEE Transactions on Power Electronics. Copyright © IEEE.**

Effects of Magnetic Coupling of Nonadjacent Resonators on Wireless Power Domino-Resonator Systems

Chi Kwan Lee, *Member, IEEE*, W. X. Zhong, and S. Y. R. Hui, *Fellow, IEEE*

Abstract—In this paper, the effects of the magnetic coupling of nonadjacent resonators on the optimal frequency of wireless power transfer are addressed. A power analysis has been carried out to identify the adjacent and nonadjacent power flow components. It is found that such cross-coupling effects of nonadjacent resonators would cause the maximum efficiency operation to slightly shift away from the resonance frequency of the resonators. Theoretical reasons for such phenomena are provided and experimentally confirmed with practical measurements in a wireless power transfer system comprising several magnetically coupled resonators arranged in a straight domino form.

Index Terms—Electromagnetic coupling, magnetic induction, wireless power transfer.

I. INTRODUCTION

MAGNETICALLY coupled resonators, each comprising a coil in series with a capacitor, were used for wireless power transfer by Tesla a century ago. Tesla has demonstrated that, for a pair of magnetically coupled resonators with one used as a transmitting unit and the other as receiving unit, optimal wireless power transfer could occur at the resonance frequency of the resonators [1]. In fact, short-range wireless energy transfer via magnetically coupled coils has been widely used in electric machines since the dc and ac electric machines were invented [2], [3]. For low-power applications, wireless power transfer has found applications in battery charging for portable electronic products such as (fixed-positioning charging) electric toothbrush and medical equipment [4], [5] and (free-positioning) Qi-compatible wireless charging system for portable electronic products such as mobile phones [6]–[12]. Medium- and high-power wireless power transfer also resurfaced since 1990 when inductive power transfer techniques were investigated for industrial robots and electric vehicles [13]–[21], [32].
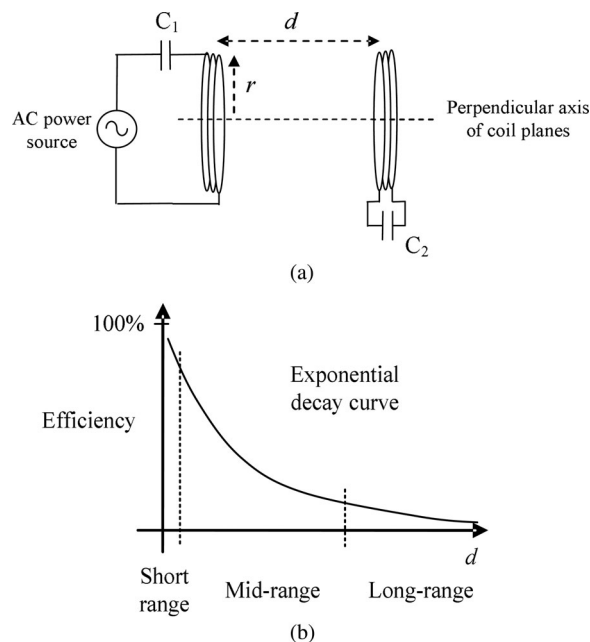
Fig. 1. (a) A pair of L-C loop resonators for wireless power transfer proposed by Tesla. (b) Typical exponential decay curve of the efficiency as a function of transmission distance *d* for wireless power transfer.

Before the recent use of a pair of Tesla's magnetically coupled resonators in [22], [23] for mid-range wireless power transfer, a series of coupled resonators operating at hundreds of Mega-Hertz have been studied for waveguide applications [24], [25]. Recently, an extra relay resonator has been inserted between the transmitting coil and the receiving coil in order to increase the energy efficiency in the wireless power transmission [26]. It has been previously pointed out [27], [28] that the energy efficiency of wireless power transfer will decrease rapidly as the transmission distance increases. For power transfer by induction, high operating frequency will increase the ac winding resistance and, therefore, decrease the energy efficiency of the resonator system. Such high-frequency winding loss is particularly relevant when high-power applications, such as induction heating, are involved [29], [30]. In order to reduce the cost of the high-frequency voltage source and reduce the ac winding resistance, sub-Mega-Hertz operation is chosen in this study for achieving high quality factor (which affects the mutual coupling) and energy efficiency. The use of the relay resonator serves the purpose of utilizing an operating point of high energy efficiency as indicated in Fig. 1.

Since the Tesla's work, these wireless power transfer studies utilize the resonance frequency of the resonators. In this paper, we present an analysis on a wireless power system comprising multiple relay resonators between the transmitting and receiving units. We show that, once relay resonators are introduced, the magnetic coupling of nonadjacent resonators would shift the optimal operating point for maximum energy efficiency away from the resonance frequency of the resonators. Theoretical results highlighting this phenomenon will first be provided. Then practical measurements are included to verify this theoretical finding.

II. BASIC CIRCUIT MODEL AND OPTIMIZATION METHOD

Modeling of the domino-resonator system is not new and can be done by using standard coupled circuit theory commonly employed in electric machines [2], [3] and magneto-inductive resonator system [23], [24]. For a domino-resonator system consisting of n-coupled resonators shown in Fig. 2, the general circuit equations can be expressed by (1), as shown at the bottom of the next page, where $M_{ij} = k_{ij}\sqrt{L_i L_j}(i, j = 1, 2, \ldots, n; i \neq j)$ is the mutual inductance between winding-i and winding-j, k_{ij} is magnetic coupling coefficient between winding-i and winding-j, R_L is the load resistance which is connected to winding-n, C_{ne} is the equivalent capacitance of the load and the compensating capacitor of winding-n which could be connected in series or parallel with the load.

$$I_1 = I_s \sin(\omega t) \qquad (2)$$
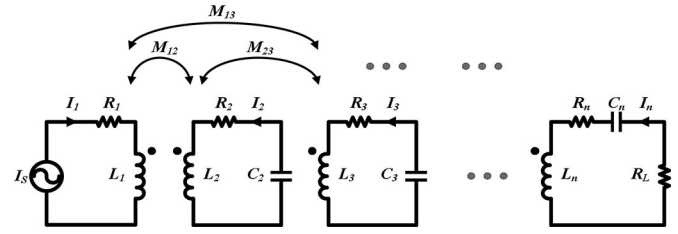
where I_s is an ac excitation current source.

Fig. 2. Schematic of a system with n resonators.

Other variables are

I_i: Current in winding-i.
L_i: Self-inductance of winding-i.
C_i: Compensating capacitance of winding-i. which is the sum of the parasitic capacitance of the winding and the externally added capacitor (if any).
R_i: Resistance in resonator -i (sum of the resistance of winding-i and the equivalent series resistance of the capacitor C_i).
ω: Angular frequency.

It should be noted that the model equation (1) represents a general system that is not restricted to resonance-frequency operation. The efficiency of the n-winding system can be expressed in (3), as shown at the bottom of the page.

All the terms I_m/I_n ($m = 1, 2, \ldots, n-1$) in (3) can be obtained from (1) and $I_1 = I_s \sin(\omega t)$. With the parameters of the resonators given, i.e., L_i, C_i, and R_i ($i = 1, 2, \ldots, n$), the efficiency can be further expressed by a function

$$\eta = f(\omega, M_{12}, M_{13}, \ldots, M_{(n-1)n}, R_L). \qquad (4)$$

$$
\begin{bmatrix}
j\omega M_{12} & R_2 + j\left(\omega L_2 - \dfrac{1}{\omega C_2}\right) & j\omega M_{23} & \cdots & \cdots & j\omega M_{2n} \\
j\omega M_{13} & j\omega M_{23} & R_3 + j\left(\omega L_3 - \dfrac{1}{\omega C_3}\right) & \cdots & \cdots & j\omega M_{3n} \\
\vdots & \vdots & \vdots & \ddots & \vdots & \vdots \\
j\omega M_{1(n-1)} & \cdots & \cdots & R_{n-1} + j\left(\omega L_{n-1} - \dfrac{1}{\omega C_{n-1}}\right) & j\omega M_{(n-1)n} \\
j\omega M_{1n} & \cdots & & & j\omega M_{(n-1)n} & \begin{array}{c} R_n + R_L + j \\ \times \left(\omega L_n - \dfrac{1}{\omega C_{ne}}\right) \end{array}
\end{bmatrix}
$$

$$
\cdot
\begin{bmatrix}
\mathbf{I}_1 \\ \mathbf{I}_2 \\ \vdots \\ \mathbf{I}_{n-1} \\ \mathbf{I}_n
\end{bmatrix}
= \mathbf{0}. \qquad (1)
$$

$$
\eta = \frac{I_n^2 R_L}{I_1^2 R_1 + I_2^2 R_2 + \cdots + I_n^2 (R_n + R_L)}
$$
$$
= \frac{R_L}{(I_1/I_n)^2 R_1 + (I_2/I_n)^2 R_2 + \cdots + (I_{n-1}/I_n)^2 R_{n-1} + R_n + R_L}. \qquad (3)
$$

In a straight domino resonator system, the mutual inductances between every two windings could be worked out with the distances between the windings provided that the geometries of the windings are given. Thus, we can obtain the expression of the energy efficiency as a function of the operation frequency, the distances of every two adjacent windings and the load as

$$\eta = f(\omega, d_{12}, d_{23}, \ldots, d_{(n-1)n}, R_L) \tag{5}$$

Then, optimization can be carried out based on (5). The constraint needed is the total transmission distance d_{total}

$$d_{12} + d_{23} + \cdots + d_{(n-1)n} = d_{\text{total}} \tag{6}$$

In this study, we use circular windings. For two coaxial circular filamentary current loops, Maxwell [31] has derived a well-known equation to calculate the mutual inductance:

$$M = \mu_0 \frac{\sqrt{r_1 r_2}}{g} [(2 - g^2)\mathbf{K}(g) - 2\mathbf{E}(g)] \tag{7}$$

where $\mathbf{K}(g)$ and $\mathbf{E}(g)$ are complete elliptic integrals of the first and second kind, respectively, and

$$g = \sqrt{\frac{4r_1 r_2}{d^2 + (r_1 + r_2)^2}} \tag{8}$$

where r_1, r_2, and d are the radius of loop-*1*, loop-*2*, and the distance between them, respectively.

For two coaxial circular thin-wall windings, the mutual inductance can be calculated by

$$M = \sum_{i=1}^{n_1} \sum_{j=1}^{n_2} M_{ij}. \tag{9}$$

III. POWER FLOW ANALYSIS BASED ON PRACTICAL RESONATORS

Since the use of relay resonators in the short-range regime could increase the overall wireless power transmission efficiency, the effects of the mutual coupling of nonadjacent resonators cannot be ignored. In this section, we present a power flow analysis that identifies the power flow paths and their equations with such cross-coupling effects included. This analysis technique provides a tool for us to study the effects of the cross-coupling of the nonadjacent resonators in any wireless power domino-resonator systems.

Practical resonators have been built for various experiments. Theoretical studies have been conducted based on the parameters of the practical resonators, which are listed in Table I. It should be noted that in the following analysis and experiments, the compensating capacitor of the last resonator is connected in series with the load; however, the parallel compensation is also common in practice. The transformation between parallel compensation and series compensation can be worked out using the following equation:

$$\frac{R_{Lp}/(j\omega C_p)}{R_{Lp} + 1/(j\omega C_p)} = \frac{R_{Ls} + 1}{(j\omega C_s)} \tag{10}$$

TABLE I
PARAMETERS OF THE PRACTICAL RESONATORS

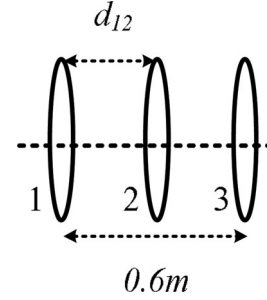| Radii of the winding	155mm	Layers of the wire	1
Number of turns	11	Length of the winding	15mm
Structure of the wire	Ø0.12mm×50strands Outer Ø1.2mm	Inductance	90.7μH
Capacitance	1.036nF (Sum of the external capacitor and the parasitic capacitance of the winding)	Resistance (at 520kHz)	0.9 Ω

Fig. 3. A *3*-resonator system with total transmission distance of 0.6 m. [Note: Resonator-*1* is the transmitter unit and resonator-*3* the receiver unit.]

where R_{Lp} and C_p are the load resistance and the parallel connected capacitor values, respectively, when the last resonator is parallel compensated; R_{Ls} and C_s are the load resistance and the series-connected capacitor values, respectively, when the last resonator is series-compensated.

A. Methodology for Power-Flow Analysis

The methodology of the power-flow analysis is demonstrated with the use of a *3*-resonator system (with one relay resonator inserted between the transmitting and receiving units), as shown in Fig. 3. In this example, there are two power paths in the *3*-resonator system. The first path involves adjacent resonators *1* and *2* and adjacent resonators *2* and *3* (*1-2-3*). The other path involves nonadjacent resonators *1* and *3* (*1-3*), i.e., the cross-coupling path.

The power flow in each path can be worked out in order to understand how the power flows will change under frequency variation. First, the relationships between the winding currents can be determined by solving (1) for the *3*-resonator system as

$$\frac{\mathbf{I}_2}{\mathbf{I}_1} = \frac{-\omega M_{12} R_{\text{out}} + j(\omega^2 M_{13} M_{23} - \omega M_{12} X_3)}{R_2 X_3 + R_{\text{out}} X_2 + j(X_2 X_3 - R_2 R_{\text{out}} - \omega^2 M_{23}^2)} \tag{11}$$

$$\frac{\mathbf{I}_3}{\mathbf{I}_1} = \frac{-\omega M_{13} R_2 + j(\omega^2 M_{12} M_{23} - \omega M_{13} X_2)}{R_2 X_3 + R_{\text{out}} X_2 + j(X_2 X_3 - R_2 R_{\text{out}} - \omega^2 M_{23}^2)} \tag{12}$$

where $X_2 = \omega L_2 - 1/(\omega C_2)$; $X_3 = \omega L_3 - 1/(\omega C_3)$; $R_{\text{out}} = R_3 + R_L$.

Now assuming the input current is 1A, with the help of (11) and (12), the complex power flows can be expressed as

(13)–(15) as shown at the bottom of this page.

$$\mathbf{S}_3 = P_3 + jQ_3 = |\mathbf{I_3}|^2 (R_{\text{out}} + jX_3)$$

$$= \frac{\omega^2 M_{13}^2 R_2^2 + (\omega^2 M_{12} M_{23} - \omega M_{13} X_2)^2}{(R_2 X_3 + R_{\text{out}} X_2)^2 + (X_2 X_3 - R_2 R_{\text{out}} - \omega^2 M_{23}^2)^2}$$

$$\times (R_{\text{out}} + jX_3)$$

$$= \mathbf{S}_{23} + \mathbf{S}_{13} \tag{16}$$

where $\mathbf{S}_{ij}(i, j = 1, 2, 3)$ represents the complex power generated in resonator-j due to the current in resonator-i and $\mathbf{S}_3$ represents the total complex power in resonator-3.

B. Effects of Mutual Coupling of Nonadjacent Resonators in an Equally Spaced 3-Resonator System

In our initial study, the three resonators are equally spaced with total transmission distance of 0.6 m and load resistance is 10 Ω. The details of the resonators are given in Table I. In order to highlight the effects of the cross-coupling of the nonadjacent resonators, the individual power-flow curves and the overall energy efficiency without and with the inclusion of the mutual magnetic couplings of the 3-resonator system are plotted as a function of operating frequency in Fig. 4(a) and (b), respectively. The natural resonance frequency of the resonator (i.e., 519.2 kHz) is chosen as the base value for the operating frequency. It can be seen that

1) Without considering the cross-coupling of nonadjacent resonators-1 and 3, the power flow curves of P_{12} and P_{23} are near symmetrical around the resonance frequency and the maximum efficiency occurs at the resonance frequency of the resonator [Fig. 4(a)]. (This is in line with Tesla's observation on 2-resonator systems when the resonators-1 and 3 were kept far apart.)

2) With the cross-coupling of nonadjacent resonators included, it can be seen from Fig. 4(b) that the power flow curves of P_{12}, P_{23}, and P_{13} are no longer symmetrical around the resonance frequency. P_{13} is close to zero at resonance frequency, positive below the resonance frequency and negative above the resonance frequency. The maximum points of P_{12} and P_{23} occur below the resonance frequency.

3) The consequence of the inclusion of the cross-coupling of nonadjacent resonators-1 and 3 is that the maximum efficiency operation occurs slightly below the resonance frequency in this 3-resonator system.

The analysis provides some physical insights into these observations. At the resonance frequency, the cross-coupled power flow P_{13} in the path 1-3 approaches zero. The reason can be deduced from the following equations of the system:

$$j\omega M_{12} \mathbf{I_1} + R_2 \mathbf{I_2} + j\omega M_{23} \mathbf{I_3} = 0 \tag{17}$$

$$j\omega M_{13} \mathbf{I_1} + j\omega M_{23} \mathbf{I_2} + (R_3 + R_L) \mathbf{I_3} = 0. \tag{18}$$

From (17) and (18),

$$\mathbf{I_3} = -\frac{\omega^2 M_{12} M_{23} + j\omega M_{13} R_2}{\omega^2 M_{23}^2 + R_2(R_3 + R_L)} \mathbf{I_1}. \tag{19}$$

$$\mathbf{S_{12}} = P_{12} + jQ_{12} = -j\omega M_{12} \mathbf{I_1} \mathbf{I_2^*}$$

$$= \frac{\left(\begin{pmatrix} \omega^2 M_{12}^2 X_3 R_2 X_3 + \omega^2 M_{12}^2 R_{\text{out}}^2 R_2 + \omega^4 M_{12}^2 M_{23}^2 R_{\text{out}} \\ -\omega^3 M_{12} M_{13} M_{23} R_2 X_3 - \omega^3 M_{12} M_{13} M_{23} R_{\text{out}} X_2 \end{pmatrix} \atop +j \begin{pmatrix} \omega^3 M_{12} M_{13} M_{23} X_2 X_3 + \omega^4 M_{12}^2 M_{23}^2 X_3 - \omega^5 M_{12} M_{13} M_{23}^3 \\ -\omega^3 M_{12} M_{13} M_{23} R_2 R_{\text{out}} - \omega^2 M_{12}^2 R_{\text{out}}^2 X_2 - \omega^2 M_{12}^2 X_3 X_2 X_3 \end{pmatrix} \right)}{(R_2 X_3 + R_{\text{out}} X_2)^2 + (X_2 X_3 - R_2 R_{\text{out}} - \omega^2 M_{23}^2)^2} \tag{13}$$

$$\mathbf{S_{23}} = P_{23} + jQ_{23} = -j\omega M_{23} \mathbf{I_2} \mathbf{I_3^*}$$

$$= \frac{\left(\begin{pmatrix} \omega^3 M_{12} M_{23} M_{13} R_2 X_3 + \omega^4 M_{12}^2 M_{23}^2 R_{\text{out}} \\ -\omega^3 M_{12} M_{23} M_{13} R_{\text{out}} X_2 - \omega^4 M_{13}^2 M_{23}^2 R_2 \end{pmatrix} \atop +j \begin{pmatrix} \omega^5 M_{12} M_{23}^3 M_{13} + \omega^3 M_{12} M_{23} M_{13} X_2 X_3 \\ -\omega^3 M_{12} M_{23} M_{13} R_{\text{out}} R_2 - \omega^4 M_{12}^2 M_{23}^2 X_3 - \omega^4 M_{13}^2 M_{23}^2 M_{13} X_2 \end{pmatrix} \right)}{(R_2 X_3 + R_{\text{out}} X_2)^2 + (X_2 X_3 - R_2 R_{\text{out}} - \omega^2 M_{23}^2)^2} \tag{14}$$

$$\mathbf{S_{13}} = P_{13} + jQ_{13} = -j\omega M_{13} \mathbf{I_1} \mathbf{I_3^*}$$

$$= \frac{\left(\begin{pmatrix} \omega^2 M_{13}^2 R_2^2 R_{\text{out}} + \omega^4 M_{23}^2 M_{13}^2 R_2 + \omega^2 M_{13}^2 R_{\text{out}} X_2^2 \\ -\omega^3 M_{12} M_{23} M_{13} R_2 X_3 - \omega^3 M_{12} M_{23} M_{13} R_{\text{out}} X_2 \end{pmatrix} \atop +j \begin{pmatrix} \omega^2 M_{13}^2 R_2^2 X_3 + \omega^2 M_{13}^2 X_2^2 X_3 + \omega^3 M_{12} M_{23} M_{13} R_2 R_{\text{out}} \\ +\omega^5 M_{12} M_{23}^3 M_{13} - \omega^3 M_{12} M_{23} M_{13} X_2 X_3 - \omega^4 M_{23}^2 M_{13}^2 X_2 \end{pmatrix} \right)}{(R_2 X_3 + R_{\text{out}} X_2)^2 + (X_2 X_3 - R_2 R_{\text{out}} - \omega^2 M_{23}^2)^2} \tag{15}$$
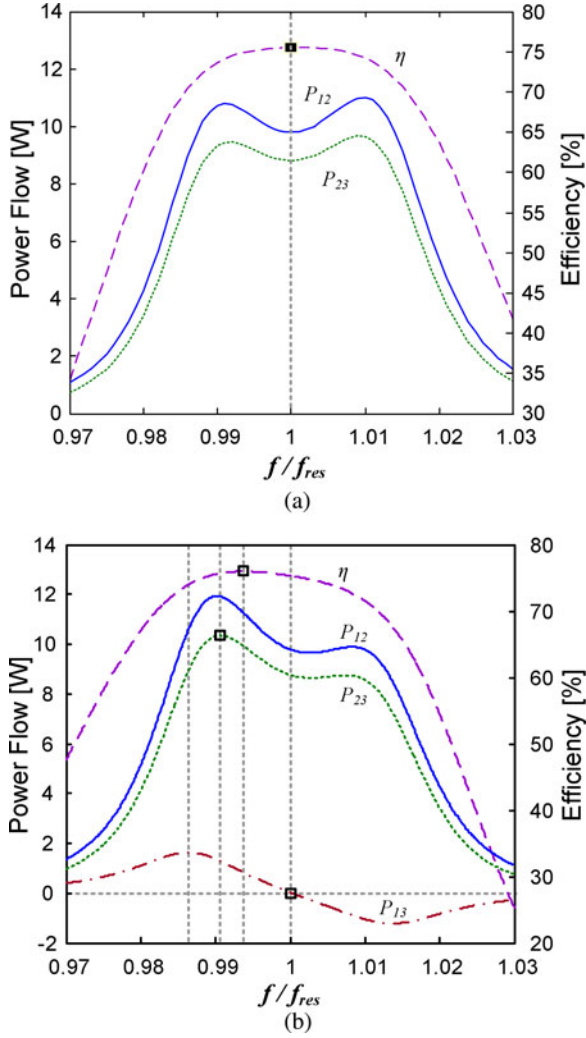
Fig. 4. (a) Variations of power flow and energy efficiency with operating frequency of an equally spaced *3*-resonator system in a straight domino arrangement, *excluding* the effects of mutual coupling of nonadjacent resonators. [Note: Frequency is normalized by the resonance frequency.] (b) Variations of power flow and energy efficiency with operating frequency of an equally spaced *3*-resonator system in a straight domino arrangement, *including* the effects of mutual coupling of nonadjacent resonators.

TABLE II
POWER FLOW OF THE *3*-RESONATOR SYSTEM UNDER DIFFERENT FREQUENCIES

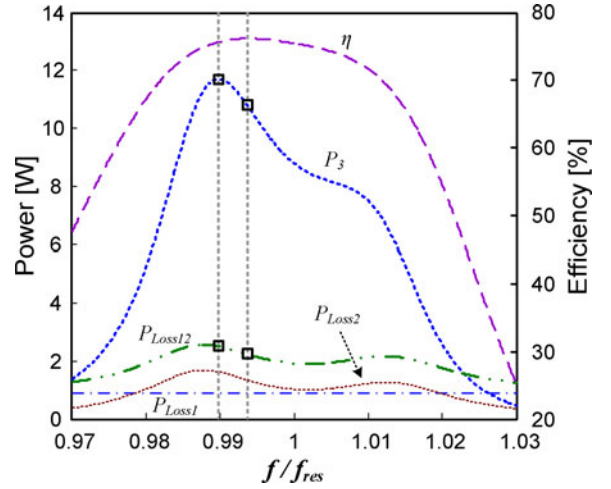| f/f_{res}	0.9864	0.9906	0.9937	1
η (purple curve) [%]	73.99	75.70	75.99	75.23
P_{12} [W]	10.61	11.92	11.27	9.794
P_{23} [W]	8.97	10.35	9.936	8.766
P_{13} [W]	1.626	1.299	0.8421	0.0281
η_2 [%] (P_{23}/P_{12})	84.54	86.83	88.16	89.50

Fig. 5. Total power delivered to the receiving resonator (P_3) and the power losses on resonator-*1* and *2* of the equally spaced *3*-resonator system as a function of frequency.

In the equally spaced *3*-resonator system described above, $M_{12} = M_{23} = 2.857 \times 10^{-6}$H, $M_{13} = 5.326 \times 10^{-7}$H thereby,

$$\frac{\omega^2 M_{12} M_{23}}{\omega M_{13} R_2} = 55.55. \tag{20}$$

Since $\omega^2 M_{12} M_{23} \gg \omega M_{13} R_2$

$$\mathbf{I_3} \approx -\frac{\omega^2 M^2}{\omega^2 M^2 + (R_3 + R_L)R_2}\mathbf{I_1}. \tag{21}$$

Therefore, the currents in resonator-*3* and *1* are essentially out of phase and, therefore, the complex power $(jM_{13}\mathbf{I_1}) \cdot \mathbf{I_3^*}$ delivered from resonator-*1* to resonator-*3* directly contains reactive power only. This deduction is valid for the systems in which the distance between nonadjacent resonators is relatively large (e.g., larger than twice the diameter of the resonator coil).

The maximum efficiency of the system will be achieved only when both of the power flow paths (i.e., the path via adjacent resonators and the path via nonadjacent resonators) are optimally utilized. In Fig. 4(b), the four vertical dotted lines indicate four special frequencies which are, from right to left, the resonant frequency and the frequencies at which the maximum values of η, P_{23}, and P_{13}, respectively, occur. Theoretical values at these four frequencies are tabulated in Table II. At the resonance frequency, the power flow via nonadjacent resonators (P_{13}) is virtually zero, meaning that all the power must flow through the relay resonator (i.e., the adjacent resonator path). Therefore, it is not the most efficient operation because the cross-coupling path via the nonadjacent resonators is not utilized. This situation is in some way analogous to power flow through two parallel resistors. No matter how large one of the resistors is, it will always reduce the overall resistance. In this case, the nonadjacent resonator path 1-3 has relatively large impedance due to the small mutual inductance. Nevertheless, it still provides positive power flow slightly below the resonance frequency to increase the overall performance of the system.

The overall energy efficiency of the system also can be expressed as

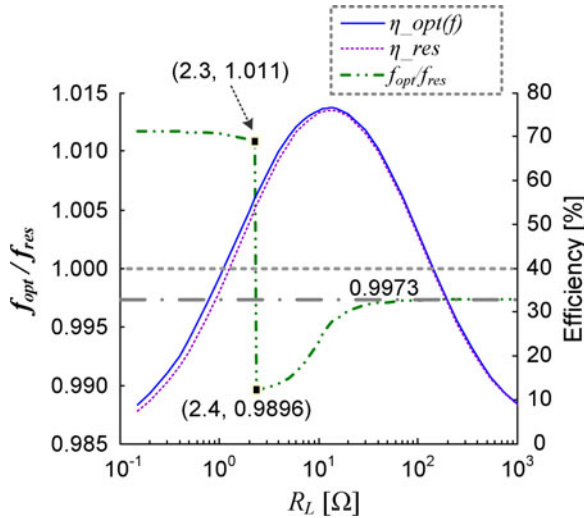$$\eta = \frac{P_3}{P_{in}}\eta_3 = \frac{P_3}{P_3 + P_{Loss12}} \cdot \frac{R_L}{R_3 + R_L} \tag{22}$$

Fig. 6. Optimum frequency and efficiency curves of the equally spaced *3*-resonator system with a wide range of load values. $\eta\_opt(f)$ and η_res represent the efficiency curve with the operation frequencies optimized and the resonant frequency, respectively. $f_{\mathrm{opt}}/f_{\mathrm{res}}$ represent the curve of the optimum frequency normalized by the resonant frequency.

Fig. 7. Optimal frequency and efficiency curves of the *3*-resonator system with optimized distances and a wide range of load values. $\eta\_opt(f, d)$ represents the efficiency curve with the operating frequency and the spacing optimized, and η_res represents the efficiency curve under the resonant frequency. $f_{\mathrm{opt}}/f_{\mathrm{res}}$ represents the curve of the optimal frequency normalized by the resonant frequency.

where P_3 is the total power delivered to the receiving resonator, P_{in} is the input power, η_3 is the energy efficiency of resonator-*3* and $P_{\mathrm{Loss}12}$ is the total power loss on resonator-*1* and *2*. It is clear that η_3 is constant for a given receiving resonator and a load resistor. For a given set of R_L and R_3, the energy efficiency of the system is decided by P_3 and $P_{\mathrm{Loss}12}$. Fig. 5 shows the variations of P_3 and the energy efficiency η. $P_{\mathrm{Loss}1}$ and $P_{\mathrm{Loss}2}$ are the power losses on resonator-*1* and *2*, respectively. At the frequency ($f/f_{\mathrm{res}} = 0.9898$) where P_3 reaches its peak, P_3 is 11.71 W and $P_{\mathrm{Loss}12}$ is 2.517 W ($P_{\mathrm{Loss}12}/P_3 = 2.517/11.71 = 0.215$). While at optimum frequency ($f/f_{\mathrm{res}} = 0.9937$), P_3 is 10.78 W and $P_{\mathrm{Loss}12}$ is 2.234 W ($P_{\mathrm{Loss}12}/P_3 = 2.234/10.78 = 0.207$).

Fig. 6 shows the optimum frequency (normalized by the resonance frequency and optimized for maximum energy efficiency operation) and the energy efficiency of the system under a wide range of resistive load values in the case study of the *3*-resoantor system. The optimum frequency is slightly higher than resonance frequency when R_L is very small (heavy load) and it will change sharply to be lower than the resonance frequency when the load changes from 2.3 Ω to 2.4 Ω. Beyond 2.4 Ω, the optimum frequency will increase gradually to a constant which is about 0.9973 times the resonant frequency.

Generally, the efficiency improvements using the optimum-frequency operation over the resonance-frequency operation are more apparent when R_L is small and the optimum frequencies have relatively large differences from the resonance frequency. The difference of energy efficiency between the optimum-frequency and the resonance-frequency operation in this *3*-resonator system is quite small because the effects arising from the crosscoupling between nonadjacent resonators is fairly small in this case. However, when the number of resonators increases and the total transmission distance decreases,
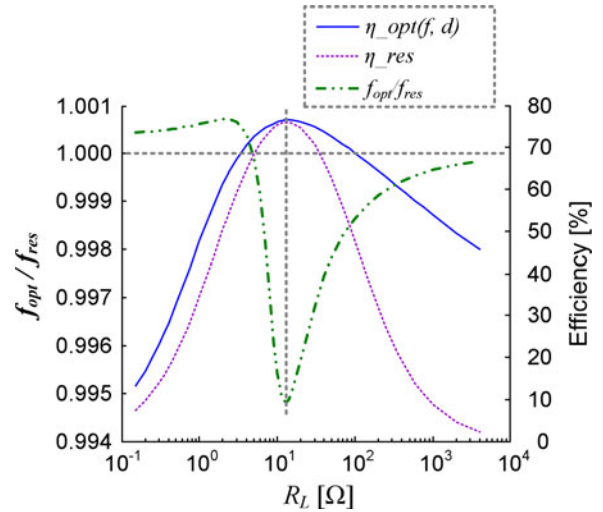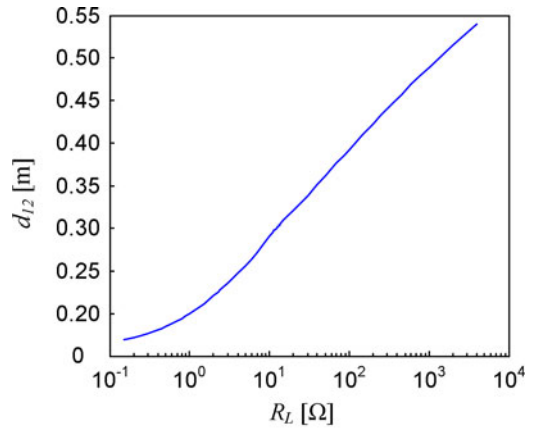

Fig. 8. Variation of the optimal distance between the 1st and 2nd resonators (d_{12}) of a *3*-resonator system (with an overall transmission of 0.6 m) for a wide range of load values at the optimized frequencies.

such cross-coupling effects will become more obvious as will be demonstrated later.

C. Effects of Mutual Coupling of Nonadjacent Resonators in an Optimally Spaced 3-Resonator System

In order to find out the optimal operation condition for a given domino system, the spacing between the resonators should also be considered. Based on an optimization algorithm, the spacing of the resonators for a given overall transmission distance can be determined if the objective of the optimization is to maximize the energy efficiency [18]. Fig. 7 shows the energy efficiency curve of the *3*-resonator system with both the operating frequency and distances among resonators optimized. The efficiency curve at the resonance frequency is also included in Fig. 7 for comparison. It can be observed that the energy efficiency can be improved over a wider load range if both of the
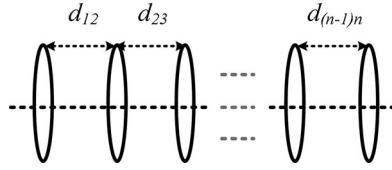
Fig. 9.   General domino-system with *n* resonators.

operating frequency and spacing are optimized. The normalized optimal frequency curve ($f_{\mathrm{opt}}/f_{\mathrm{res}}$) is also plotted in Fig. 7. It is noted that the optimal frequency can be higher or lower than the resonance frequency depending on the load and that a slight shift from the resonance frequency could affect the efficiency significantly.

For this *3*-resonator system with an overall transmission distance of 0.6 m, the variation of the optimal spacing between the first and the second resonators with a range of resistive load is plotted in Fig. 8. If maximum energy efficiency is set as the objective, it is noted that the relay resonator (i.e., resonator-*2*) should be placed closer to resonator-*1* for a heavy load (i.e., small R_L) and closer to resonator-*3* when the load is light (i.e. large R_L).

From the above analysis of the *3*-resonator system with total transmission distance of 0.6 m, we get a better understanding of how the three parameters (f, d_{12}, R_L) affect the power transmission efficiency of the system simultaneously. In this particular case, the optimal operation point for maximum efficiency could be found at the conditions of ($f/f_{\mathrm{res}}, d_{12}, R_L$) = (0.9949, 0.306 m, 14.07 Ω). However, the system model presented in Section II can be used for other objective functions such as maximization of power transfer.

D. Effects of Mutual Coupling of Nonadjacent Resonators in Optimally Spaced n-Resonator Systems

The general model in Section II can be used to optimize the domino systems with more resonators, as shown in Fig. 9. In this part of the analysis, the investigation is extended to an *n*-resonator domino system. Two conditions are considered here:

1) Based on a fixed "average distance" d_e between two adjacent resonators, the performance of the straight domino-resonator systems as a function of the number of resonators is observed. For a straight *n*-resonator system, the total transmission distance d_{total} equals to $(n-1)d_e$. For example, $d_{\mathrm{total}} = 2d_e$ for a *3*-resonator system.
2) Based on a fixed number of resonators, the performance of the *n*-resonator system as a function of the total transmission distance d_{total} is investigated.

In both conditions, the equally and optimally spaced systems are studied and compared. For the equally spaced systems, the objective is to maximize the efficiency function, with the load as an optimized variable, subject to the constraints of equally spaced resonators and resonance frequency operation as follows:

Max: $\eta(R_L)$
With: $d_{12} = d_{23} = \ldots = d_{(n-1)n} = d_e = d_{\mathrm{total}}/(n-1)$
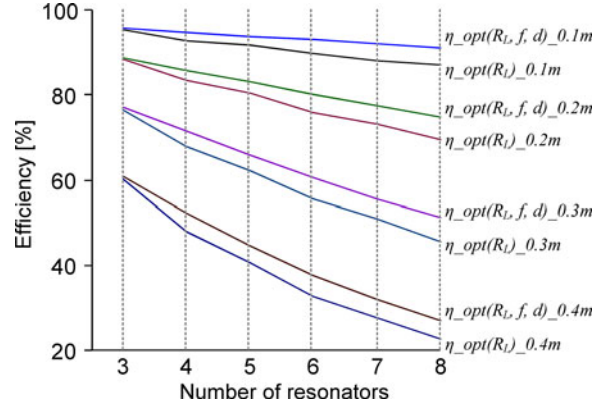$\qquad f = f_0$

Fig. 10.   Efficiency comparison between the domino systems with loads, frequencies, and distances optimized ($\eta_{\_\mathrm{opt}}(R_L, f, d)$) and the equally spaced systems operating at resonant frequency and with only loads optimized ($\eta_{\_\mathrm{opt}}(R_L)$) for four different average distances: 0.1 m, 0.2 m, 0.3 m, and 0.4 m.
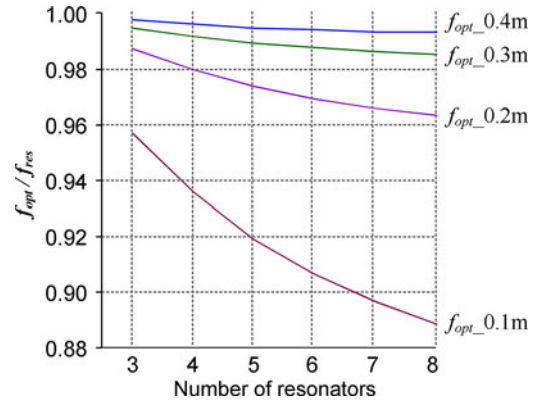

Fig. 11.   Optimized frequency normalized by resonant frequency as a function of the number of resonators.
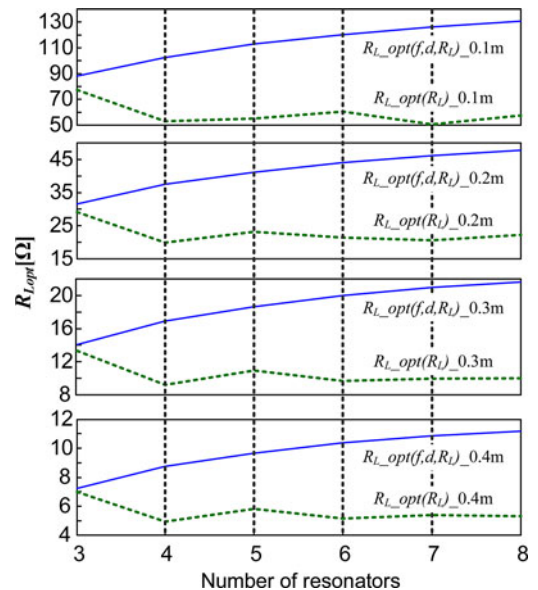

Fig. 12.   Variations of the optimum load values for the two sets of optimization criteria as a function of the number of resonators.
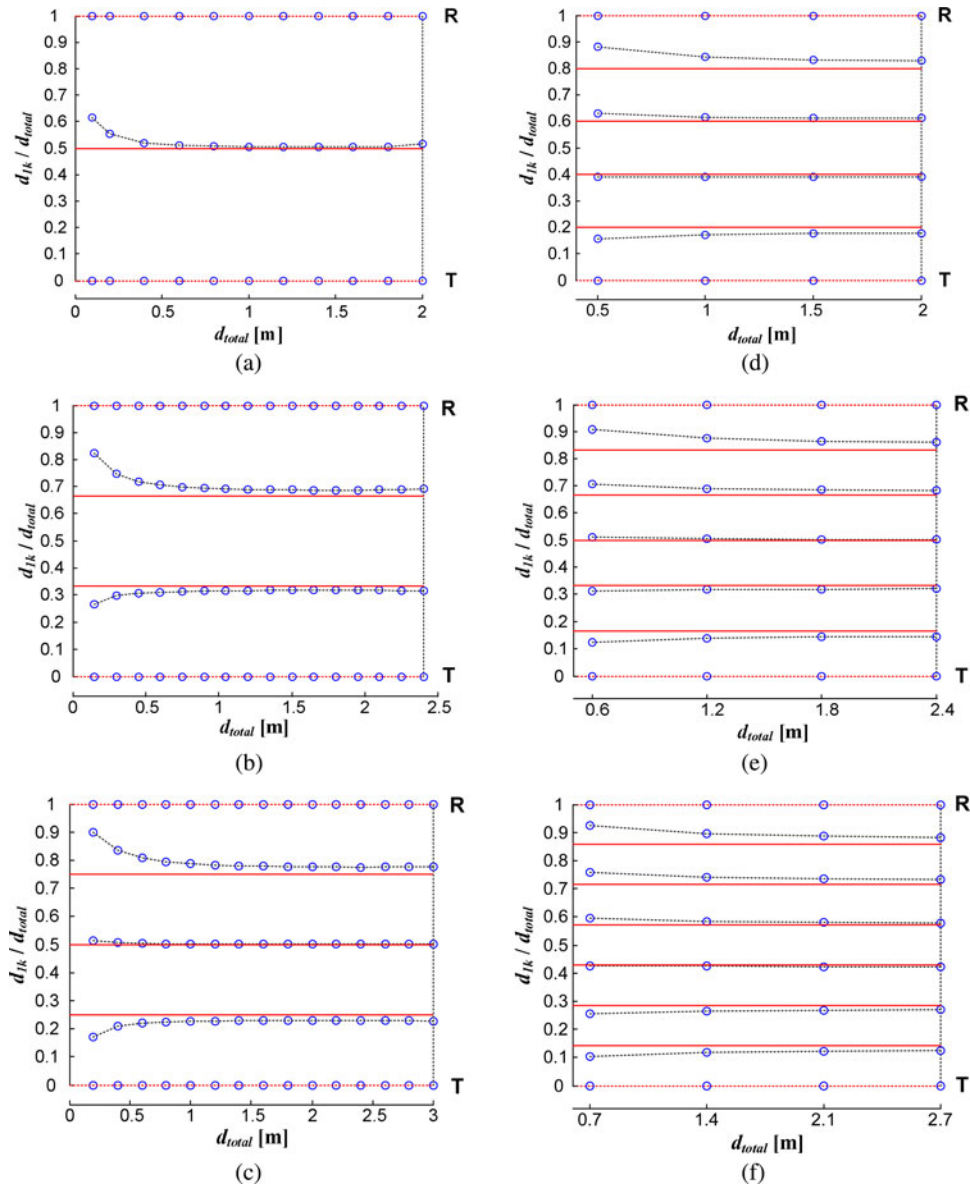
Fig. 13.   Equal and optimal spacing of the resonators in the domino systems. The red solid lines indicate the positions for the equally-spaced resonators and the blue circles indicate the positions for the optimal-spaced resonators.

where d_{total} is the total transmission distance, d_e is the average distance, and f_0 is the resonance frequency of the resonators.

For the optimally spaced systems, the objective is to maximize the energy efficiency, with the operating frequency, the spacing between adjacent resonators and the load as optimized variables, subject to a certain overall transmission distance as follows:

Maximize: $\eta(R_L, f, d_{12}, d_{23}, \ldots, d_{(n-1)n})$
Subject to: $d_{12} + d_{23} + \cdots + d_{(n-1)n} = d_{\text{total}}$.

1) Fixed Average Distance: The systems with average distances of $0.1\,\text{m}$, $0.2\,\text{m}$, $0.3\,\text{m}$, and $0.4\,\text{m}$ are examined for straight domino resonators with the number of resonators ranging from 3 to 8. Fig. 10 shows the comparison of the energy efficiency curves based on the two sets of optimization criteria

for these four averaged distances. Two important points can be observed:

1) As expected, the energy efficiency is higher when the averaged distance and hence the overall transmission distance is smaller.

2) Regardless of the overall transmission distance and the number of resonators, the systems with the operating frequency, spacing and load optimized consistently outperform those with only load optimized at resonance frequency operation in terms of energy efficiency. That is, $\eta_{\_\text{opt}}(R_L, f, d)$ is higher than $\eta_{\_\text{opt}}(R_L)$ in all cases. This observation indicates that equally spaced systems operated at the resonance frequency are not the optimal systems in terms of maximizing efficiency when relay resonators are used. The shift of the operating frequency at which
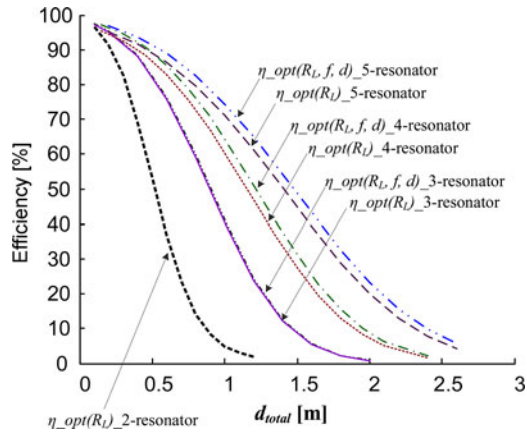
Fig. 14. Efficiency comparison between the domino systems for the *2-*, *3-*, *4-*, and *5*-resonator systems for a range of the total transmission distances.

Fig. 15. Optimum operation frequencies of the domino systems with loads, frequencies, and distances optimized as a function of the total transmission distance.

Fig. 16. Optimum loads of the domino systems with loads, frequencies, and distances optimized as a function of the total transmission distance.
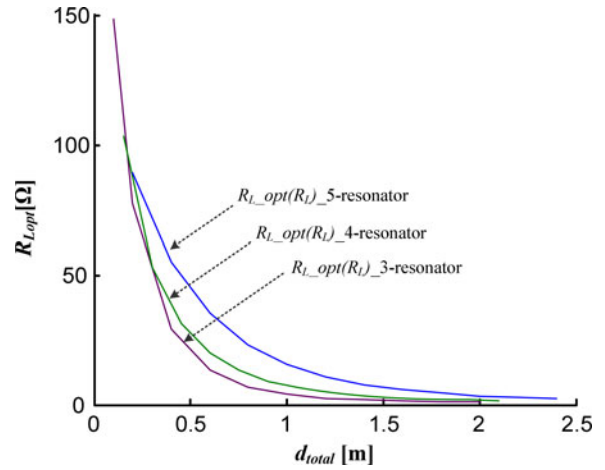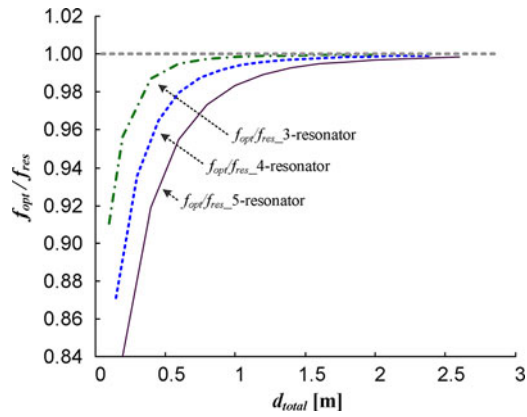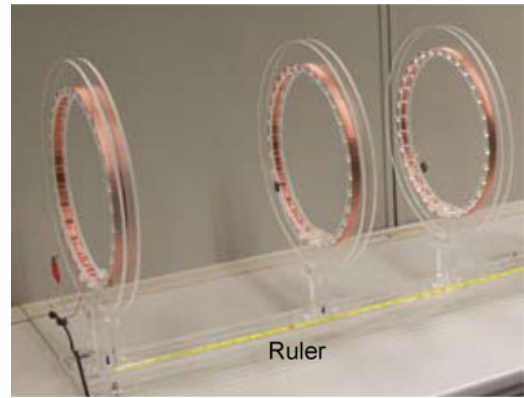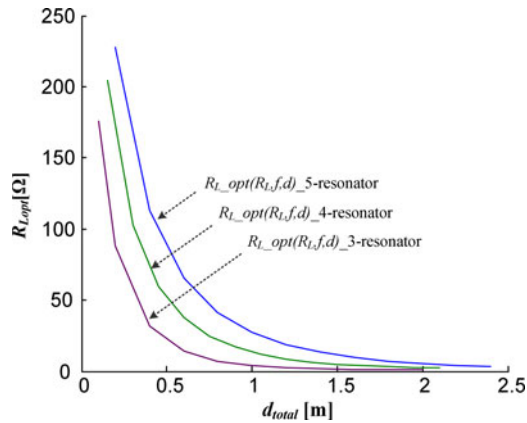

Fig. 17. Optimum loads of the equally spaced domino systems operating at the resonant frequency with only loads optimized.

Fig. 18. A practical 3-resonator domino-system.

Fig. 19 Measured (upper) and simulated (lower) current waveforms of an equally spaced *3*-resonator system operating at the resonance frequency of 519.2 kHz (1 A/Div., 500 ns/Div.).

maximum efficiency occurs can be explained from the cross-coupling effect as explained previously.

The variations of the four optimal frequency curves as a function of the number of resonators are plotted in Fig. 11. It is important to note that the optimal frequencies occur below the resonance frequency for their respective optimized loads. It is also
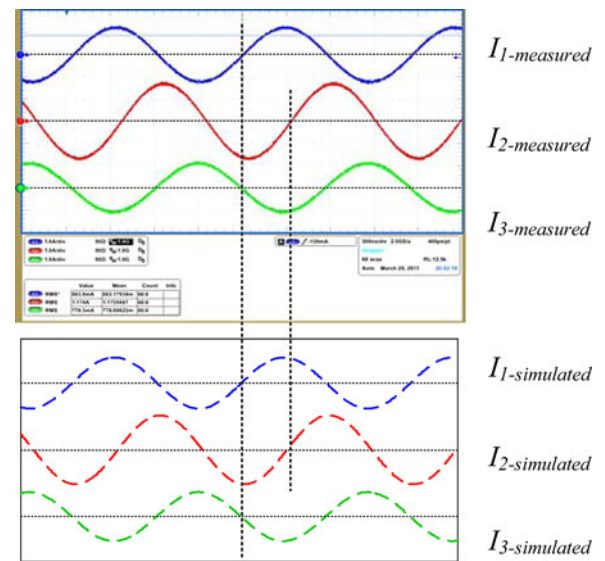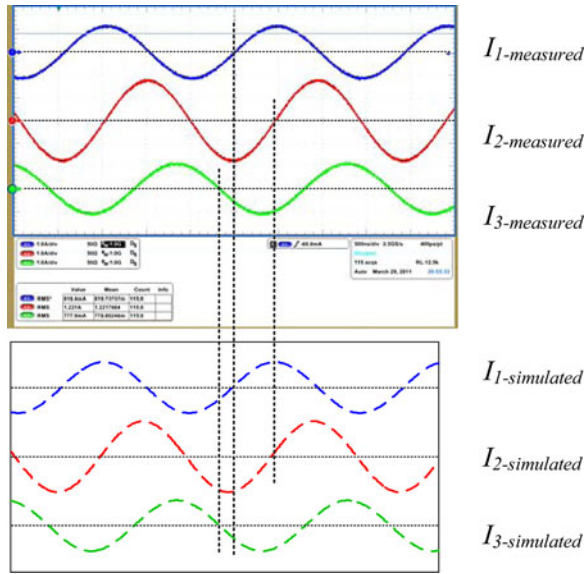
Fig. 20. Measured (upper) and simulated (lower) current waveforms of an equally spaced *3*-resonator system operating at 516.7 kHz, slightly below the resonance frequency (1 A/Div., 500ns/Div.).
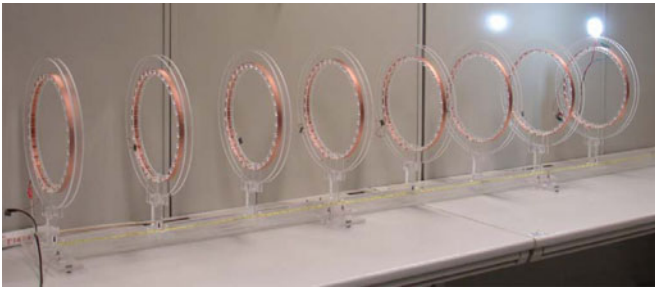

Fig. 21 Photograph of the experimental setup of an *8*-resonator system powering an 18 W compact fluorescent lamp over a distance of 2.1 m.

TABLE III
THEORETICAL AND MEASURED VALUES FOR OPTIMUM FREQUENCIES AND CORRESPONDING MAXIMUM EFFICIENCY

	Theoretical f_{opt} [kHz]	Measured f_{opt} [kHz]	Theoretical η_{max} [%]	Measured η_{max} [%]	Theoretical R_{Lopt} [Ω]	Practical R_{Lopt} [Ω]
5-resonator equal-spaced	517.3	517.5	61.86	61.18	10.1	10.0
5-resonator optimized-distances	513.6	513.5	64.96	65.19	18.7	18.4
6-resonator equal-spaced	514.9	515.0	56.44	55.18	11.3	11.1
6-resonator optimized-distances	512.7	513.0	59.60	60.40	20.0	19.7

is that distance between resonator-$(n - 1)$ and resonator-n is smaller than the distance between resonator-*1* and resonator-*2* (i.e., $d_{(n-1)n} < d_{12}$), and both of them are smaller than average distances (i.e., $d_{12} < d_e$ and $d_{(n-1n)} < d_e$).

2) Fixed Number of Resonators: The results for the study based on fixed number of resonators are recorded in Figs. 14–17. In Fig. 14, the efficiency curves are plotted against the total transmission distance for the domino systems with *3*-, *4*-, and *5*-resonators. It can be seen that, for a given transmission distance, the use of more relay resonators can increase the efficiency. Also the optimally spaced resonator systems offer higher efficiency than equally spaced resonator systems.

For the scheme that allows the operating frequency to be optimized, the normalized optimal frequency curves for the *3*-, *4*-, and *5*-resonator systems under consideration are plotted in Fig. 15. Similar conclusion can be drawn from Fig. 15 as from Fig. 11, that is, the optimal frequency of the system with a higher number of resonators and a shorter total transmission distance deviates more from the resonance frequency. The corresponding optimal load values for the scheme with the load, frequency, and spacing optimized are included in Fig. 16, while those for the scheme operated at the resonance frequency with only the load optimized are shown in Fig. 17.

IV. PRACTICAL VERIFICATION

Experiments have been carried out to verify the analysis using a few straight domino-resonator systems. A practical setup of *3*-resonator domino system is shown in Fig. 18. Pure resistive loads are used to do the measurements. In order to check the validity of the model and the analysis, the measured resonator currents of this *3*-resonator system are captured and compared with the simulated results. The measured and theoretical resonator currents for the equally spaced *3*-resonator system operating at the resonance frequency 519.2 kHz (resonance frequency of the resonators) are shown in Fig. 19. The total transmission distance d_{total} is 0.6 m and d_{12} is 0.3 m. The theoretical results agree very well with the measurements. In particular, it is noted that I_3 is 180° out of phase with I_1 as predicted in (21). The measured and theoretical current waveforms obtained at the optimal frequency of 516.7 kHz (which is lower than the resonance frequency) are shown in Fig. 20. Again, they agree well and I_1 and I_3 have a phase shift of about 150° against a theoretical phase shift of 153°. The measured efficiency at 519.2 kHz is 75.17% while that at 516.7 kHz is 75.74%.

More relay resonators can be added to increase the overall transmission distance. Fig. 21 shows a photograph of an

noted that the deviation from the resonance frequency increases as the averaged distance between resonators decrease and the number of resonators increases. With a smaller overall distance and a larger number of resonators, the cross-coupling paths between nonadjacent resonators become more effective and so the optimal frequency shift further away from the resonance frequency. For example, if eight optimally spaced resonators are used for an overall distance of 0.7 m, the optimal frequency f_{opt}_0.1 m is about 0.89 times the resonance frequency. On the other hand, if three optimally spaced resonators are used for an overall distance of 0.8 m, the optimal frequency f_{opt}_0.4 m approaches the resonance frequency. The corresponding variations of the optimized load resistance are included in Fig. 12.

If the overall distance d_{total} between the transmitter resonator (labeled as **T**) and receiving resonator (labeled as **R**) is normalized as one, the relative positions of the equally spaced and optimally spaced relay resonators for the cases of using three to eight resonators are plotted in Fig. 13(a) to (f). It is noted that the optimum spacing starts to share a similar pattern when the average distances are large enough which makes the effect of the width of the coils small. One obvious feature of the patterns
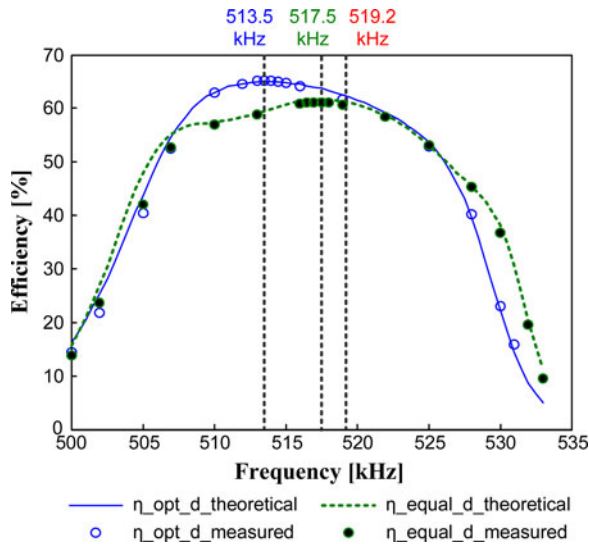
Fig. 22. Measured and theoretical efficiency of the equally spaced and optimally spaced 5-resonator systems.
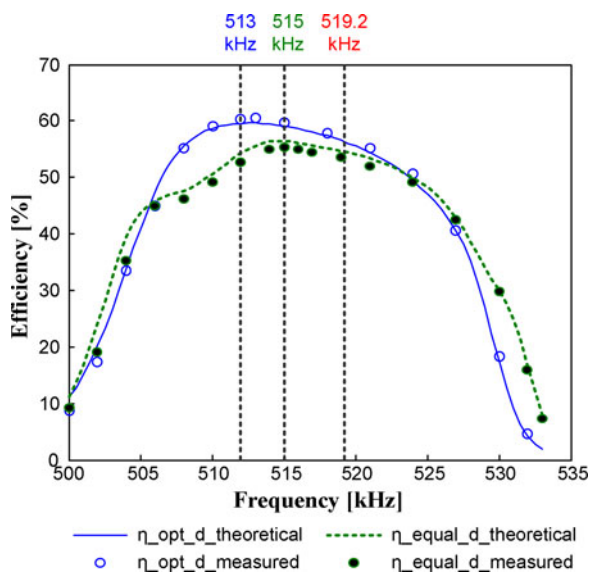

Fig. 23. Measured and theoretical efficiency of the equally spaced and optimally spaced 6-resonator systems.

8-resonator system wirelessly transmitting power to light up a 14 W compact fluorescent lamp over a distance of 2.1 m. In order to practically confirm the effects of the mutual coupling of the nonadjacent resonators, both measured and theoretical results of a 5-resonator and 6-resonator systems under the two sets of optimization criteria are included in Table III. For the equally spaced systems, the spacing between adjacent resonators is fixed at 0.3 m. For the optimallyspaced 5-resonator and 6-resonator systems, the spacing arrangements are (0.273 m, 0.328 m, 0.338 m, 0.261 m) and (0.264 m, 0.322 m, 0.333 m, 0.330 m, 0.251 m), respectively.

The theoretical energy efficiency curves and their practical measurements for the 5-resonator system are shown in Fig. 22. It can be seen that the theoretical predictions are highly consistent with the practical measurements. Higher energy efficiency can be achieved by the optimally spaced system and the maximum efficiency occurs at a frequency (513.5 kHz), which is slightly below the resonance frequency of 519.2 kHz. Similar set of theoretical and practical results are included in Fig. 23 for a 6-resonator system. The operating frequency of the maximum efficiency of the optimally spaced scheme now occurs at 513 kHz. The shift of the optimal operating frequency from the resonance frequency due to the mutual magnetic coupling of the nonadjacent resonators is confirmed by these experiments.

V. CONCLUSION

In this paper, we use the well-established magnetic coupled circuit model to investigate the effects of the magnetic coupling of nonadjacent resonators for wireless power transfer applications. As verified by the analysis and practical measurements, the cross-coupling effects of the nonadjacent resonators cause the optimal frequencies for both the equally spaced and the optimally spaced resonator systems to shift away slightly from the resonance frequency of the resonators. The efficiency improvements by using the optimally spaced systems operating at the optimal frequencies could be more than 3% in the 5-resonator and 6-resonator systems when compared with equally spaced systems operated at the resonance frequency. The cross-coupling effects of the nonadjacent resonators increase with increasing number of resonators and decreasing spacing between adjacent resonators. The analytical approach presented here has been favorably verified by practical measurements. It can be used to study wireless power transfer systems based on the use of resonators arranged in domino forms.

REFERENCES

[1] R. Lomas, *The man who invented the twentieth century – Nikola Tesla – Forgotten Genius of Electricity*. London, U.K: Headline Book Publishing Ltd., 1999, p. 146.
[2] C. V. Jones, *The Unified Theory of Electrical Machines.*. London, U.K: Butterworths, 1967.
[3] M. G. Say, *Alternating Current Machines*, 4th ed. New York: Pitman, 1976.
[4] K. Oguri, "Power supply coupler for battery charger," US Patent 6 356 049, 2000.
[5] Y. Yang, and M. Jovanovic, "Contactless electrical energy transmission system," US Patent 6 301 128, 2000.
[6] H. J. Brockmann and H. Turtiainen, "Charger with inductive power transmission for batteries in a mobile electrical device," US Patent 6 118 249, 1999.
[7] B. Choi, J. Nho, H. Cha, T. Ahn, and S. Choi, "Design and implementation of low-profile contactless battery charger using planar printed circuit board windings as energy transfer device," *IEEE Trans. Ind. Electron.*, vol. 51, no. 1, pp. 140–147, Feb. 2004.
[8] Y. Jang and M. M. Jovanovic, "A contactless electrical energy transmission system for portable-telephone battery chargers," *IEEE Trans. Ind. Electron.*, vol. 50, no. 3, pp. 520–527, Jun. 2003.
[9] C.-G. Kim, D.-H. Seo, J.-S. You, J.-H. Park, and B. H. Cho, "Design of a contactless battery charger for cellular phone," *IEEE Trans. Ind. Electron.*, vol. 48, no. 6, pp. 1238–1247, Dec. 2001.
[10] S. Y. R. Hui and W. C. Ho, "A new generation of universal contactless battery charging platform for portable consumer electronic equipment," *IEEE Trans. Power Electron.*, vol. 20, no. 3, pp. 620–627, May 2005.

[11] X. Liu and S. Y. R. Hui, "Simulation study and experimental verification of a contactless battery charging platform with localized charging features," *IEEE Trans. Power Electron.*, vol. 22, no. 6, pp. 2202–2210, Nov. 2007.

[12] S. Y. R. Hui, "Planar inductive battery charging system," US Patent 7576514, 2009.

[13] Albert Esser, "Contactless charging and communication for electric vehicles," *IEEE Ind. Appl. Mag.*, vol. 1, no. 6, pp. 4–11, Nov./Dec. 1995.

[14] T. Imura, H. Okabe, and Y. Hori, "Basic experimental study on helical antennas of wireless power transfer for electric vehicles by using magnetic resonant couplings," in *Proc. IEEE Vehicle Power Propulsion Conf.*, 2009, Dearborn, MI, pp. 936–940.

[15] Y. Hori, "Future vehicle society based on electric motor, capacitor and wireless power supply," in *Proc. 2010 Int. Power Electron. Conf. (IPEC)*, Sapporo, Japan, Jun. 21–24, pp. 2930–2934.

[16] K. Sugimori and H. Nishimura, "A novel contact-less battery charger for electric vehicles," in *Proc. 29th Annu. IEEE Power Electron. Spec. Conf.*, May. 1998, vol. 1, pp. 559–564.

[17] H. H. Wu, J. T. Boys, and G. A. Covic, "An AC processing pickup for IPT systems," *IEEE Trans. Power Electron.*, vol. 25, no. 5, pp. 1275–1284, May 2010.

[18] H. L. Li, A. P. Hu, G. A. Covic, and C. S. Tang, "Optimal coupling condition of IPT system for achieving maximum power transfer," *Electron. Lett.*, vol. 45, no. 1, pp. 76–77, 2009.

[19] A. P. Hu, C. Liu, and H. L. Li, "A novel contactless battery charging system for soccer playing robot," in *Proc. 15th Int. Conf. Mechatronics Machine Vision Practice*, Auckland, NZ, Dec. 2–4, 2008, pp. 646–650.

[20] G. A. Covic, J. T. Boys, M. L. G. Kissin, and H. G. Lu, "A three-phase inductive power transfer system for roadway-powered vehicles," *IEEE Trans. Ind. Electron.*, vol. 54, no. 6, pp. 3370–3378, Dec. 2007.

[21] Z. Pantic, S. Bhattacharya, and S. Lukic, "Optimal resonant tank design considerations for primary track compensation in inductive power transfer systems," in *Proc. IEEE Energy Convers. Congr. Exposition (ECCE)*, Sep. 2010, pp. 1602–1609.

[22] A. Karalis, J. D. Joannopoulos, M. Soljacic, "Wireless energy transfer," US Patent 7825543, Nov. 2010.

[23] A. Kurs, A. Karalis, R. Moffatt, J. D. Joannopoulos, P. Fisher, and M. Soljačić, "Wireless power transfer via strongly coupled magnetic resonances," *Science*, vol. 317, pp. 83–86, 6 Jul. 2007.

[24] R. R. A. Syms, E. Shamonina, and L. Solymar, "Magneto-inductive waveguide devices," *IEE Proc. Microw., Antennas Propagation*, vol. 153, no. 2, pp. 111–121, Apr. 2006.

[25] R. R. A. Syms, E. Shamonina, and L. Solymar, "A theory of metamaterials based on periodically loaded transmission lines: Interaction between magnetoinductive and electromagnetic waves," *J. Appl. Phys.*, vol. 97, p. 064909, 2005.

[26] F. Zhang, S. Hackworth, W. Fu, and M. Sun, "The relay effect on wireless power transfer using witricity," in *Proc. IEEE Conf. Electromagn. Field Comput.*, May. 9–12, 2010, Chicago, MA.

[27] E. Waffenschmidt and T. Staring, "Limitation of inductive power transfer for consumer applications," in *Proc. Eur. Conf. Power Electron. Appl.*, 2009, Sep. 8–10, Barcelona, Spain, pp. 1–10.

[28] J. O. Mur-Miranda, G. Fanti, F. Yifei, K. Omanakuttan, R. Ongie, A. Setjoadi, and N. Sharpe, "Wireless power transfer using weakly coupled magnetostatic resonators," in *Proc. 2010 IEEE Energy Conversion Congress and Exposition (ECCE)*, Atlanta, GA, Sep. 12–16, 2010, pp. 4179–4186.

[29] J. Acero, C. Carretero, I. Millan, O. Lucia, R. Alonso, and J. M. Burdio, "Analysis and modeling of planar concentric windings forming adaptable-diameter burners for induction heating appliances," *IEEE Trans. Power Electron.*, vol. 26, no. 5, pp. 1546–1558, May 2011.

[30] C. Carretero, J. Acero, R. Alonso, J. M. Burdio, and F. Monterde, "Embedded ring-type inductors modeling with application to induction heating systems," *IEEE Trans. Magn.*, vol. 45, no. 12, pp. 5333–5343, Dec. 2009.

[31] J. C. Maxwell, *A Treatise on Electricity and Magnetism.* New York: Dover, 1954 (reprint from the original from 1873).

[32] H. H. Wu, G. A. Covic, J. T. Boys, and D. J. Robertson, "A series-tuned inductive-power-transfer pickup with a controllable ac-voltage output," *IEEE Trans. Power Electron.*, vol. 26, no. 1, pp. 98–109, Jan. 2011.

Chi Kwan Lee (M'08) received the B.Eng. and Ph.D. degrees in electronic engineering from the City University of Hong Kong, Kowloon, Hong Kong, in 1999 and 2004, respectively.

He was a Postdoctoral Research Fellow in the Power and Energy Research Centre at the National University of Ireland, Galway, Ireland, from 2004 to 2005. In 2006, he joined the Centre of Power Electronics in City University of Hong Kong, as a Research Fellow. In 2008–2011, he was a Lecturer in the Electrical Engineering Department at the Hong Kong Polytechnic University, Hong Kong. Since 2012, he has been an Assistant Professor with the Department of Electrical and Electronic Engineering, The University of Hong Kong.

His current research interests include applications of power electronics to power systems, advanced inverters for renewable energy and smart grid applications, reactive power control for load management in renewable energy systems, wireless power transfer, energy harvesting, and planar electromagnetics for high frequency power converters.

W. X. Zhong was born in China, in 1984. He received the B.S. degree in electrical engineering from Tsinghua University, Beijing, China, in 2007. He is currently working toward his Ph.D. degree at the Center for Power Electronics, City University of Hong Kong, Hong Kong.

His current research interests include synchronous rectification and wireless power transfer.
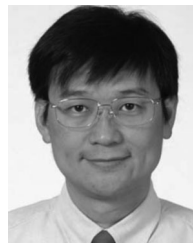
S. Y. R. Hui (M'87–SM'94–F'03) received the Ph.D. degree at Imperial College London, U.K., in 1987.

He has previously held academic positions at the University of Nottingham, the University of Sydney, and City University of Hong Kong. He joined the University of Hong Kong as Chair Professor in 2011. Concurrently, he has held the Chair Professorship at Imperial College London since 2010. He has published more than 200 technical papers, including more than 150 refereed journal publications and book chapters. More than 50 of his patents have been adopted by industry. He has been an Associate Editor of the IEEE TRANSACTIONS ON POWER ELECTRONICS, since 1997, and an Associate Editor of the IEEE TRANSACTIONS ON INDUSTRIAL ELECTRONICS, since 2007. He has been appointed twice as an IEEE Distinguished Lecturer by the IEEE Power Electronics Society, in 2004 and 2006. He served as one of the 18 Administrative Committee members of the IEEE Power Electronics Society and was the Chairman of its Constitution and Bylaws Committee from 2002 to 2010. He received the Excellent Teaching Award at CityU, in 1998, and the Earth Champion Award, in 2008. He won an IEEE Best Paper Award from the IEEE IAS Committee on Production and Applications of Light, in 2002, and two IEEE Power Electronics Transactions Prize Paper Awards for his publications on Wireless Battery Charging Platform Technology, in 2009, and on LED system theory, in 2010. His inventions on wireless charging platform technology underpin key dimensions of Qi, the world's first wireless power standard, with freedom of positioning and localized charging features for wireless charging of consumer electronics. In November 2010, he received the IEEE Rudolf Chope R&D Award from the IEEE Industrial Electronics Society, and the IET Achievement Medal (The Crompton Medal).

Prof. Hui is a Fellow of the IET and the Australian Academy of Technological Sciences and Engineering.